Corrosion behavior of Ti_3AlC_2 in NaOH and H_2SO_4 ☆

Dan Li [a,b], Ying Liang [a,b], Xiaoxia Liu [a], Yanchun Zhou [b,*]

[a] *Department of Chemistry, Northeastern University, Shenyang 110819, China*
[b] *Shenyang National Laboratory for Materials Science,*
Institute of Metal Research, Chinese Academy of Sciences, 72 Wenhua Road, Shenyang 110016, China

Abstract

Passivation behavior, corrosion kinetics and film formation mechanism of Ti_3AlC_2 in 1 M NaOH and 1 M H_2SO_4 solutions were investigated by linear potential scan, electrochemical impedance spectroscopy, cyclic voltammetry, SEM and XPS. The corrosion resistance mainly depended on the formation of passivating films on Ti_3AlC_2 in 1 M NaOH and 1 M H_2SO_4, which led to different corrosion processes. Ti_3AlC_2 displayed good corrosion resistance in NaOH due to the formation of dense and protective Ti oxides as the passivating film. However, it exhibited poor corrosion resistance in H_2SO_4 which attributed to the formation of permeable Ti sub-oxides as the pseudo-passivating film.
© 2010 Elsevier Ltd. All rights reserved.

Keywords: Ti_3AlC_2; Corrosion; Electrochemical measurements; XPS

1. Introduction

The layered ternary carbides and nitrides, also called *MAX* phases (where M is an early transition metal; A is an A group element; X is C or N) have attracted attentions of material scientists, physicists and chemists due to their unique properties.[1–3] A significant number of papers concerning the structural, thermal, electrical and mechanical properties of *MAX* phases have been published up to now. However, only a few works have been done to discuss their electrochemical behaviors. Corrosion resistance of a material is very important for its potential applications in the chemical industry. For instance, Jovic and Barsoum discovered that Ti_3SiC_2 was highly stable in concentrated hydrochloric acid solution due to its low corrosion rate. Ti_3SiC_2 also exhibited the catalytic activity for hydrogen evolution.[4] Therefore, Ti_3SiC_2 can be used as anodes and/or cathodes for chlor-alkali

electrolysis. The corrosion behavior of Ti_3SiC_2 has been extensively studied.[5–9] In HCl and H_2SO_4, Ti atoms were leached out and Si atoms were in situ oxidized to form a SiO_2-based protective layer on the surface of Ti_3SiC_2 resulting in good corrosion resistance. Similarly, Ti_3GeC_2 exhibited good corrosion resistance due to the formation of passivating layer consisting of mainly GeO_2.[10] Polarization method has been used to study the electrochemical corrosion behavior of a series of *MAX* phases in H_2SO_4, HCl and NaOH.[5] The results showed that Ti-containing *MAX* phases were quite stable in all of the above solutions, except for Ti_2AlC which dissolved in 1 M HCl solution.

Ti_3AlC_2, an isotype of Ti_3SiC_2 and Ti_3GeC_2, is an important member of the Ti-containing *MAX* phases. Ti_3AlC_2 shows excellent oxidation resistance at high temperatures in air.[11–13] Table 1 lists the physical and mechanical properties of Ti_3AlC_2.[13] However, its corrosion behavior in acidic and basic solutions has not been explored.

In this work, the corrosion and passivating behaviors of Ti_3AlC_2 in 1 M NaOH and 1 M H_2SO_4 solutions were evaluated by linear potential scan, electrochemical impedance spectroscopy and cyclic voltammetry. The surface microstructures and chemical compositions after immersion in the solutions and anodic polarizations were characterized using scanning electron microscopy (SEM) and X-ray photoelectron spectroscopy (XPS).

Table 1
Typical properties of Ti_3AlC_2.[11]

Properties	Values
Theoretical density	4.25 g/cm^3
Coefficient of thermal expansion	9.0×10^{-6} K^{-1}
Electrical conductivity	2.9×10^6 Ω^{-1} m^{-1}
Temperature coefficient of resistivity	0.0031 K^{-1}
Vickers hardness	3.5 GPa
Young's modulus	297 GPa
Shear modulus	124 GPa
Compressive strength at room temperature	570 MPa
Brittle-to-ductile transition temperature under compression	$1050\,^\circ$C
Shear strength	138 MPa
Flexural strength	375 MPa
Fracture toughness	7.2 MPa m$^{1/2}$

2. Experimental procedure

2.1. Sample preparation

Bulk polycrystalline Ti_3AlC_2 samples used in this work were prepared by the solid–liquid reaction and simultaneous in situ hot pressing process which was detailed elsewhere.[11] Test coupons of 15 mm × 15 mm × 1 mm in size were cut from the as-prepared bulk Ti_3AlC_2 samples using electrical discharge method (EDM). To obtain reproducible surfaces, Ti_3AlC_2 coupons were wet-ground successively with SiC emery papers to 2000 grit. All of the coupons were ultrasonically cleaned with acetone, and then rinsed with distilled water before drying. Finally, the coupons were mounted in a PTFE electrochemical cell with 1.0 cm^2 in circular surface area of Ti_3AlC_2 contacting the corrosive solutions. The corrosive solutions, 1 M NaOH and 1 M H_2SO_4, were made from analytical grade chemicals and distilled water.

2.2. Electrochemical measurements

Electrochemical tests were performed in a CHI 660A electrochemical workstation (Chenhua Instrument Co. Ltd., Shanghai, China) with a conventional three-electrode electrochemical cell at room temperature. The platinum mesh counter electrode and the reference electrode, a saturated calomel electrode (SCE, all potentials were given *vs.* SCE except indicated), were placed in the settled position. A Luggin capillary was set between the working electrode and the reference electrode to minimize errors due to the IR drop in the electrolytes.

The open circuit potential (OCP), corresponding to the corrosion potential (E_{corr}) of Ti_3AlC_2, was recorded as a function of time for 24 h. Prior to electrochemical experiments on Ti_3AlC_2, such as linear potential scan, electrochemical impedance spectroscopy (EIS) and cyclic voltammetry (CV), the electrodes were stabilized in the solutions for 1 h. The linear potential scans were conducted from -0.25 V to 3.0 V (*vs.* OCP) at 1 and 0.167 mV/s. The impedance spectra were recorded from 10^{-2} Hz to 10 kHz with an applied potential at OCP. Cyclic voltammetry (CV) in NaOH was carried out at 50 mV/s, starting from OCP towards

-1.0 V (the first segment), then reversing to 1.0 V (the second segment) and finally going back to -1.0 V (the third segment). Only the second and the third segments were used for a whole cycle.

2.3. Microstructure observation of corrosion products

The microstructures and chemical compositions of the Ti_3AlC_2 coupons were characterized by SEM (LEO SUPRA 35, Oberkochen, Germany). XPS (VG ESCLAB 250, UK) was also used to determine the chemical compositions of Ti_3AlC_2 coupons after anodic polarization in 1 M NaOH and 1 M H_2SO_4 solutions. Peak fitting to decompose the XPS spectra, corresponding to different surface species, was performed using a Shirley background with Gauss:Lorentz of 80:20. The binding energies (BE) were calibrated with respect to the hydrocarbon contamination C 1s signal at 284.6 eV. In order to collect data about elemental composition on the surface and subsurface of the coupons, the surface of Ti_3AlC_2 was sputtered by Ar ion beam with a film removal rate of 0.2 nm/s for 10 s (sputter away the contamination on the surface) and 30 s, respectively.

3. Results

3.1. Open circuit potential

The OCP of Ti_3AlC_2 was recorded in 1 M NaOH and 1 M H_2SO_4 solutions (Fig. 1). In NaOH, the initial corrosion potential is observed around -0.64 V and rapidly positive-shifts to ca. -0.30 V. Then the corrosion potential changes slowly and remains almost constant with slight fluctuations. However, after ca. 20 h, the corrosion potential suddenly drops and then recovers to the steady state. In H_2SO_4, the corrosion potential decreases initially from ca. -0.17 V to -0.29 V and then increases gradually in the following ca. 20 h. Afterwards the corrosion potential starts to oscillate.
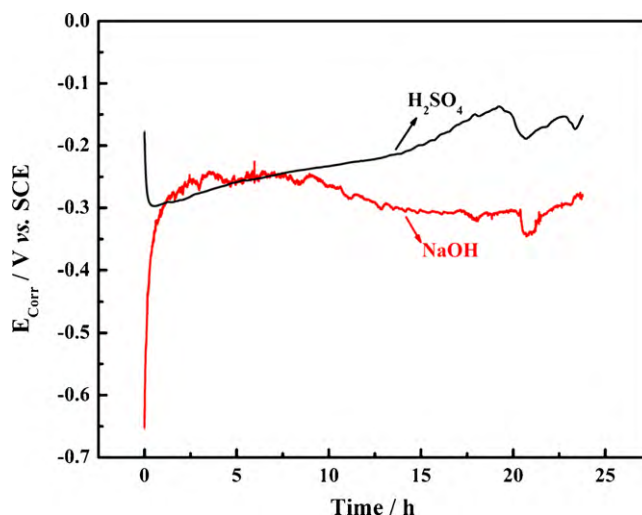
Fig. 1. Evolution of the corrosion potential of Ti_3AlC_2 as a function of time in 1 M NaOH and 1 M H_2SO_4 solutions.
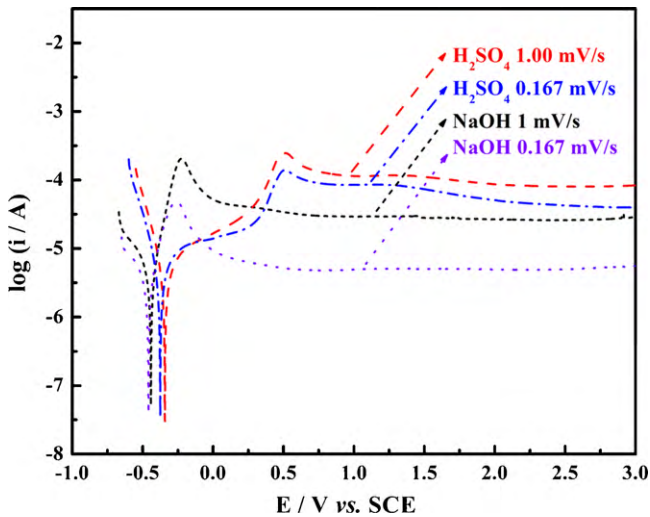
Fig. 2. Polarization curves of Ti_3AlC_2 in 1 M NaOH and 1 M H_2SO_4 solutions at the scanning rate of 1 and 0.167 mV/s, respectively.

3.2. Polarization curves

Fig. 2 presents the polarization curves of Ti_3AlC_2 in 1 M NaOH and 1 M H_2SO_4 solutions obtained by linear potential scans at 1 mV/s and 0.167 mV/s for corrosion dynamic analyses and steady state analyses, respectively. Electrochemical parameters such as corrosion potential (E_{corr}), corrosion current density (i_{corr}), Tafel constants (b_a and b_c), critical current density (i_c) and passivating current density (i_p) derived from the polarization curves are given in Table 2.

In NaOH, a short and activating region appears at the initial stage of anodic polarization as shown in Fig. 2. Then, Ti_3AlC_2 exhibits an activating-to-passivating behavior and remains in the passivating state until the end of the potential scan to 3.0 V. The passivating current density i_p at the steady state is lower than 5.00 $\mu A\,cm^{-2}$ (Table 2), while the cathodic Tafel slope b_c is more than 400 mV/dec.

In H_2SO_4, the anodic part of the polarization curve (Fig. 2) clearly reveals an inflexion at ca. −0.20 V, after that the current density increases slowly along with the anodic scan. The current density increases relatively fast from ca. −0.30 V to ca. 0.51 V, where an anodic current peak is observed. Then the current density is relative stable at 100 $\mu A\,cm^{-2}$ in the following potential scan to 3.0 V. The anodic Tafel region is not well defined, so the corrosion current density was gotten from the Tafel region of the cathodic polarization curve. Ti_3AlC_2 exhibits different behaviors in the potential range of ca. −0.2 V to 0.3 V and ca. 0.3–0.51 V, indicating different ion-transfer reactions at these two potential regions. An inconspicuous anodic oxidation peak
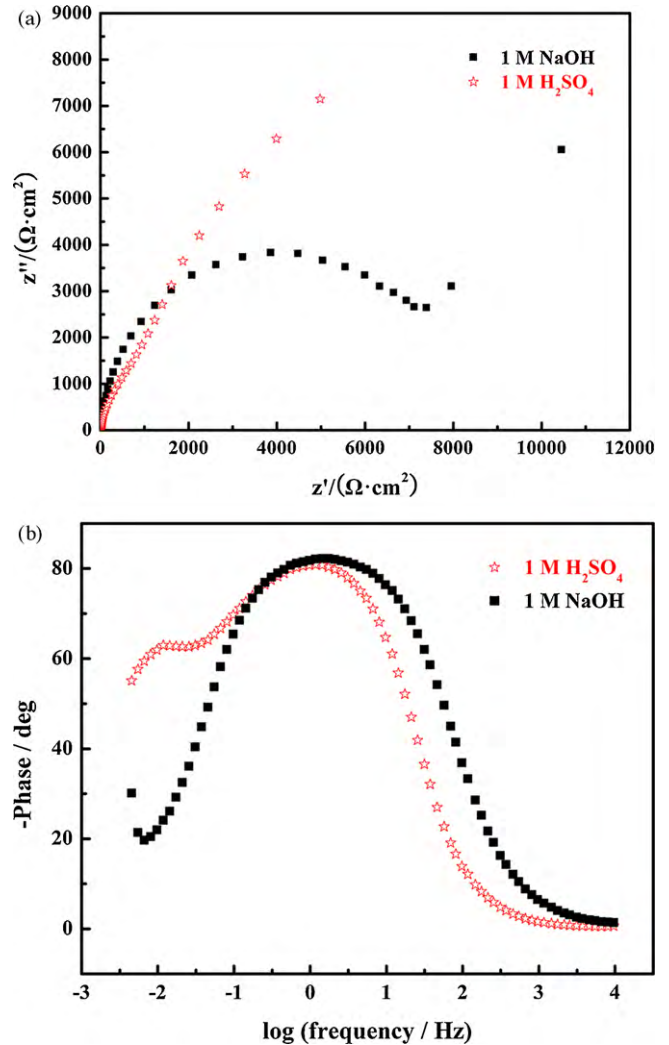
Fig. 3. Nyquist plots (a) and Bode phase angle plots (b) of Ti_3AlC_2 after 1 h immersion in 1 M NaOH (■) and 1 M H_2SO_4 (☆) solutions.

also appears at ca. 1.3 V, which possibly corresponds to oxygen evolution.

3.3. Electrochemical impedance spectroscopy (EIS)

To further investigate the corrosion process and kinetics, EIS plots of Ti_3AlC_2 were recorded in 1 M NaOH and 1 M H_2SO_4 solutions at OCP (Fig. 3). In NaOH, the Nyquist plot consists of a capacitive loop at high- and medium-frequency and an oblique line at relative low-frequency (Fig. 3(a)). The oblique line of the Nyquist plot is a typical feature of Warburg impedance, which is generally related to a Nernst diffusion of ions from the elec-

Table 2
Electrochemical parameters obtained from the polarization curves of Ti_3AlC_2 in 1 M NaOH and 1 M H_2SO_4 solutions.

Solution (1 M)	Scan rate (mV/s)	E_{corr} (V)	i_{corr} ($\mu A\,cm^{-2}$)	b_c (mV/dec)	b_a (mV/dec)	i_c ($\mu A\,cm^{-2}$)	i_p ($\mu A\,cm^{-2}$)
NaOH	1.00	−0.442	5.25	400	112	203	25.0–30.0
NaOH	0.167	−0.459	4.96	410	175	49.1	4.00–5.00
H_2SO_4	1.00	−0.343	4.51	139		246	80.0–120
H_2SO_4	0.167	−0.376	2.16	154		139	40.0–85.0
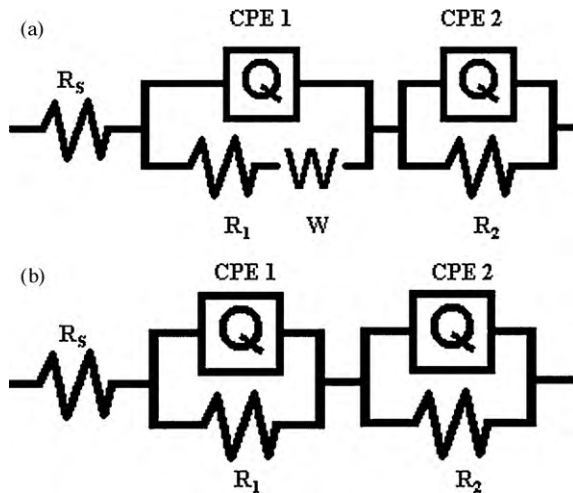
Fig. 4. Equivalent circuit of EIS for Ti_3AlC_2 after 1 h immersion in 1 M NaOH (a) and 1 M H_2SO_4 (b) solutions.

Table 3
Surface compositions of Ti_3AlC_2 after immersion in 1 M NaOH and 1 M H_2SO_4 solutions for 25 days by EDS analysis.

Element	C	O	Al	Ti	Ti:Al:C
Atomic %					
H_2SO_4	17.06		16.42	66.52	3:0.74:0.77
NaOH	8.24	43.36	9.74	38.65	3:0.76:0.64

trode to the bulk solution. It is thus concluded that the corrosion process of Ti_3AlC_2 in NaOH is controlled by ion diffusion.[14] Although the high- and medium-frequency region shows one depression arc, it actually contains two time constants.[15] This can be clearly seen from the Bode phase angle plot (Fig. 3(b)) on which a broad peak appears in the high- and medium-frequency range. An equivalent circuit as shown in Fig. 4(a) can be proposed for the EIS of Ti_3AlC_2 in NaOH, where R_s represents the solution resistance, R_1 the resistance of the passivating film, CPE1 the capacitance of the passivating film, W the Warburg resistance, while R_2 and CPE2 reflect charge-transfer resistance and double layer capacitance related to the interface of the passivating film and the solution.

In H_2SO_4, two time constants can be seen in both Nyquist plot (Fig. 3(a)) and Bode phase angle plot (Fig. 3(b)). The time constant of high-frequency region is related to the charge transfer and the second one at low-frequency range accounts for the corrosion process. The corresponding equivalent circuit is shown in Fig. 4(b), where R_s represents the solution resistance, R_1 the corrosion resistance of the pseudo-passivating film and CPE1 the pseudocapacitance, while CPE2 can be explained as double layer capacitance and R_2 refers to the charge-transfer resistance.

The capacitance here is replaced by the constant phase angle element (CPE) and described by an empirical impedance function[16]:

$$Z_{CPE} = [Y(j\omega)^n]^{-1} \tag{1}$$

where Z_{CPE} is the impedance of the constant phase element ($\Omega\, cm^2$), $j\omega$ is the complex variable for sinusoidal perturbations with

$$\omega = 2\pi f \tag{2}$$

and n is the exponent of CPE with values between -1 and 1 (n for an ideal capacitance is 1, for a pure resistance is 0 and for an inductance is -1), Y is a proportional factor that combines the properties related to both the surface and the electroactive species.[17] The presence of CPE in both NaOH and H_2SO_4 refers to the frequency dispersion of interfacial impedance, which is

attributed to the roughness and inhomogeneity of the Ti_3AlC_2 surface.[18]

3.4. Surface morphology and composition of the anodic oxidation products

To intuitively investigate the corrosion and passivating behaviors of Ti_3AlC_2 in 1 M NaOH and 1 M H_2SO_4 solutions, the surface morphologies of Ti_3AlC_2 after anodic polarization and immersion for 1 day and 25 days in the solutions were observed by SEM.

After immersion in NaOH for 1 day (Fig. 5(a)), the surface of Ti_3AlC_2 is covered by a new layer which is obviously different from the substrate (inset in Fig. 5(a)). After immersion for 25 days (Fig. 5(b)), the surface morphology is similar to that of immersion for 1 day though the surface becomes slightly rougher. These results indicate that a stable passivating film is formed on the surface of Ti_3AlC_2 after 1 day immersion and then changes little during the following days. Anodic polarization has similar effects on the surface morphology of Ti_3AlC_2 (Fig. 5(c)).

In H_2SO_4, there is no obvious change on the surface morphology of Ti_3AlC_2 after 1 day immersion (Fig. 6(a)). However, intergranular attack occurs after 25 days immersion (Fig. 6(b)) and anodic polarization (Fig. 6(c)). Non-uniform serious corrosion on grain boundaries can be clearly seen on Fig. 6(b) and (c).

The surface compositions of Ti_3AlC_2 after immersion for 25 days obtained by EDS analysis are presented in Table 3. It is shown that after immersion in both solutions, the atomic ratios of C and Al elements decrease from those of the Ti_3AlC_2 substrate. O is also detected on the EDS spectrum of the coupons immersed in NaOH, suggesting that the corrosion products in NaOH and H_2SO_4 are different.

In order to precisely determine the surface compositions of Ti_3AlC_2, XPS analysis is conducted for coupons after anodic polarization in NaOH and H_2SO_4. XPS spectra of Ti $2p_{3/2}$, Al $2p_{3/2}$ and O 1s were analyzed and the results are summarized in Tables 4 and 5, respectively.

The oxide film formed in 1 M NaOH solution consists of two layers. The outer layer consists of mainly TiO_2 (or $TiO(OH)_2$) with a small amount of Ti_2O_3 (or TiOOH), while the inner layer consists of TiO_2, Ti_2O_3 with a small amount of TiO. It is worth noting that Al is not detected in the passivating film. The anodic oxidation products formed on Ti_3AlC_2 in H_2SO_4 are quite different from those formed in NaOH. Ti sub-oxides and a few Al oxides were observed. At the same time, Al in Ti_3AlC_2 substrate can also be detected, which indicates that the anodic oxidation
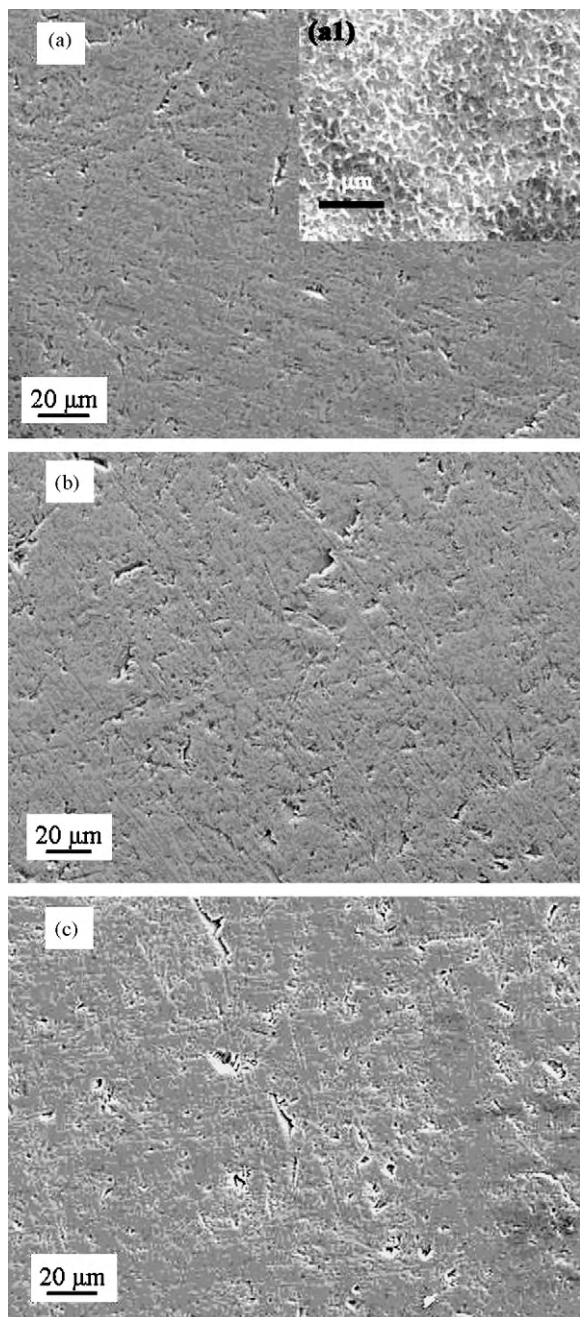
Fig. 5. Surface morphologies of Ti$_3$AlC$_2$: (a) after 1 day immersion in 1 M NaOH solution, (a1) a typical enlarge view as the inset, (b) after 25 days immersion in 1 M NaOH solution, (c) after anodic polarization from OCP to 3.0 V at the scanning rate of 0.1 mV/s in 1 M NaOH solution.

Fig. 6. Surface morphologies of Ti$_3$AlC$_2$: (a) after 1 day immersion in 1 M H$_2$SO$_4$ solution, (b) after 25 days immersion in 1 M H$_2$SO$_4$ solution, (c) after anodic polarization from OCP up to 3.0 V at the scanning rate of 0.1 mV/s in 1 M H$_2$SO$_4$ solution.

products are quite porous. Herein, no O 1s peak is detected for TiO or other oxides due to the small content.

4. Discussions

4.1. OCP

The OCP increases rapidly in NaOH indicates that instant passivation of Ti$_3$AlC$_2$ surface occurs after immersion (Fig. 1). Then Ti$_3$AlC$_2$ becomes more and more stable due to the increase

in the thickness of the passivating film, indicated by the relative stable OCP. The critical current density of the polarization curve (steady state) which is lower than 100 μA cm^{-2} in NaOH (Table 2) further demonstrates that Ti$_3$AlC$_2$ has excellent self-passivation ability.[19] So there is no significant difference in surface morphologies of Ti$_3$AlC$_2$ coupons for 1 day and 25 days immersion in NaOH. The fluctuations of the OCP curve may result from the competition between film formation and partial dissolution of corrosion products. Some unstable corrosion products also assemble on the surface of Ti$_3$AlC$_2$ so that

Table 4
Binding energies (BE) correspond to each component in the XPS spectra of the passivating layers formed on Ti_3AlC_2 electrode after anodic polarization from OCP to 3.0 V in 1 M NaOH solution, the surface was sputtered (outer layer) 10 s and (inner layer) 30 s by Ar ion beam.

Spectrum	Binding energy (eV)	FWHM (eV)	Binder energy (corresponding O 1s)
Ti_{2p} 3/2			
Outer layer species			
Ti_2O_3/TiOOH	455.7	1.99	531.1
	457.0	1.79	530.3
$TiO(OH)_2$/TiO_2	458.1	1.21	
	458.7	1.19	529.7
Inner layer species			
TiO	454.8	1.5	
Ti_2O_3	456.4	1.96	531.2
	457.9	1.37	530.3
TiO_2	458.6	1.21	529.7

severe partial dissolution also occurs. Thereafter, selective attack of the passivating film happens, which leads to the drop of the corrosion potential. Finally, the OCP recovers back to a relative stable value due to the accumulation of new corrosion products that repair the local-failure area.

It is known that a thin layer of oxides can be immediately formed on Ti_3AlC_2 when exposed to air. However, the naturally formed layer is insufficient to prevent corrosion in H_2SO_4, therefore the initial drop of OCP has been observed. As the corrosion potential of crystalline grain is higher than that of the grain boundary in H_2SO_4, preferential dissolution of grain boundaries occurs, resulting in the increase of content of crystalline grains. This intergranular corrosion should be the reason of the positive-shifts of OCP as the mixed corrosion potential is more positive. Along with this non-uniform intergranular corrosion, the surface of Ti_3AlC_2 become inhomogeneous and the OCP begins to oscillate.

4.2. Corrosion kinetics

4.2.1. Cathodic process

Based on the high cathodic Tafel constant (Table 2) in 1 M NaOH solution, it is reasonable to conclude that oxygen is transported from NaOH bulk solution to the Ti_3AlC_2 surface by a diffusion process and then diffuses through the passivating film. Thus, the cathodic process in NaOH is partially controlled by a diffusion process. The possible cathodic reaction (oxygen

absorption corrosion) is:

$$O_2 + 2H_2O + 4e^- = 4OH^- \qquad (3)$$

The cathodic Tafel constant in 1 M H_2SO_4 solution (Table 2) is much lower than that in NaOH. The corrosion in this solution should be mainly caused by the aggressive H^+, since SO_4^{2-} ions have very little corrosive effect on the material. The main cathodic reaction (hydrogen evolution corrosion) can be written by:

$$2H^+ + 2e^- = H_2 \qquad (4)$$

However, other reactions such as the reduction of oxygen cannot be ruled out.

4.2.2. Anodic process

As concluded from the EIS analysis, Ti_3AlC_2 undergoes different processes in NaOH and H_2SO_4 solutions. In 1 M NaOH solution, there are three stages for the formation and dissolution of the passivating film on Ti_3AlC_2[20]: (1) ions leach out from Ti_3AlC_2 to the passivating film, which is not generally considered as a speed-controlled step; (2) mass transfer process of the ions which occurs inside the passivating film; (3) the charge-transfer process which occurs at the interface of the passivating film and the solution. In 1 M H_2SO_4 solution, however, the corrosion products are permeable. There are possibly two steps during the corrosion process: (1) the dissolution of Ti_3AlC_2 that accounts for the corrosion process; (2) the charge-transfer pro-

Table 5
Binding energies (BE) correspond to each component in the XPS spectra of the corrosion products formed on Ti_3AlC_2 electrode after anodic polarization from OCP to 3.0 V in 1 M H_2SO_4 solution, the surface was sputtered (outer layer) 10 s by Ar ion beam.

Spectrum	Species	Binding energy (eV)	FWHM (eV)	Binding energy (corresponding O 1s)
Ti 2p 3/2	TiO	454.2	1.25	
	Ti^{n+} ($2 < n < 3$)	455.1	1.46	
	Ti_2O_3	456.2	1.46	531.2
Absorption	H_2O			532.4
Al 2p	Ti_3AlC_2	71.9	2.0	
	AlO_x	73.5	2.0	530.2
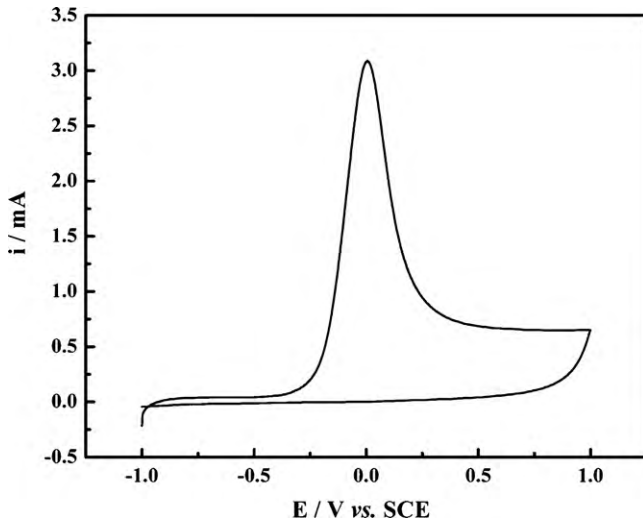
Fig. 7. Cyclic voltammogram of Ti_3AlC_2 in 1 M NaOH solution at the scanning rate of 50 mV/s.

cess that occurs at the interface of corrosion products/Ti_3AlC_2 substrate and the solution.

4.3. Film formation mechanism

In 1 M NaOH solution, the unstable anodic oxidation products such as titanium sub-oxides are partly dissolved and the stable anodic oxides such as TiO_2 accumulate as the passivating film. Titanium sub-oxides are stable at lower potentials, while TiO_2 is stable at relatively higher potentials. During the anodic potential scans starting from lower potential, the inner layer composed of compounds in lower oxidation states forms first and then the outer layer forms when scans to higher potential. In order to further shed light on the corrosion mechanism of Ti_3AlC_2 in NaOH, cyclic voltammetric scan is conducted at 50 mV/s (Fig. 7). During the scan towards the positive direction, an anodic current occurs at ca. −0.9 V, which corresponds to the formation of titanium sub-oxides, TiOOH and Ti_2O_3.[21] The current peak at ca. 0 V indicates the composition changes from Ti (III) oxide to the most stable Ti (IV) oxide.[21] Referring to the corrosion mechanism of Ti_3SiC_2,[6] anodic oxidation products of Ti_3AlC_2 in NaOH may be formed by the following reactions:

$$2Ti_3AlC_2 + 1.5O_2 = 6Ti \ (sol.) + 4C \ (sol.) + Al_2O_3 \quad (5)$$

$$Al_2O_3 + 2OH^- = 2AlO_2^- + H_2O \quad (6)$$

$$4Ti \ (sol.) + 3OH^- + 2O_2$$
$$= TiOOH + Ti_2O_3 + TiO + H_2O + 3e^- \quad (7)$$

$$Ti_2O_3 + 4OH^- = 2TiO(OH)_2 + H_2O + 4e^- \quad (8)$$

$$TiO(OH)_2 = TiO_2 + H_2O \quad (9)$$
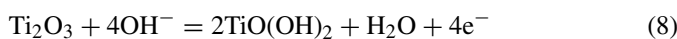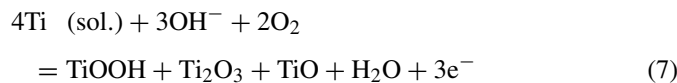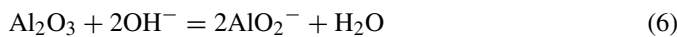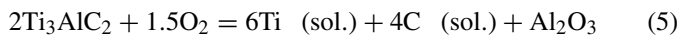
In 1 M H_2SO_4 solution, the anodic oxidation products formed on Ti_3AlC_2 are quite different from those in 1 M NaOH solution.

The corrosion reactions of Ti_3AlC_2 in H_2SO_4 can be described by:

$$Ti_3AlC_2 + 2xH^+ + 2xe^-$$
$$= 3Ti \ (sol.) + 2C \ (sol.) + Al \ (sol.) + xH_2 \ (g) \quad (10)$$

$$4Ti \ (sol.) + (x+4)H_2O$$
$$= Ti_2O_3 + TiO_x + TiO + (8+2x)H^+ + (8+2x)e^- \quad (11)$$

$$Al \ (sol.) + xH_2O = AlO_x + 2xH^+ + 2xe^- \quad (12)$$
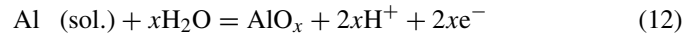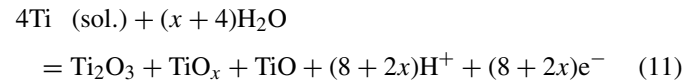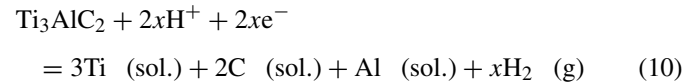
4.4. Comparison with other MAX phases

As an isotype of Ti_3SiC_2 and Ti_3GeC_2, Ti atoms should be similarly leached out from Ti_3AlC_2 in NaOH and H_2SO_4, followed by the formation of alumina-based films due to the oxidation of Al atoms. However, it is found in the present work that the formation of Ti oxides is responsible for the corrosion resistance of Ti_3AlC_2 in NaOH. Though Ti can be leached out from Ti_3AlC_2, it can immediately react with OH^- and oxygen to form Ti oxides which are tightly adsorbed on the surface of the electrode to protect Ti_3AlC_2 in NaOH. The absence of Al oxide here can be reasonably explained by the fact that Al oxide can be dissolved in NaOH to form $[Al(OH)_6]^{3-}$ or AlO_2^- ions, which agreed well with the result from the literature.[22] On the other hand, the corrosion products in H_2SO_4 that are mainly composed of Ti sub-oxides fail to protect Ti_3AlC_2 substrate since there is not enough time to form stable oxides due to the attack of H^+.

4.5. Comparison with other related materials

In order to compare corrosion behaviors of Ti_3AlC_2 with those of other related materials, the polarization curves of Ti_3AlC_2, Ti, Ti_2AlC and Ti_3SiC_2 in 1 M NaOH solution are presented in Fig. 8. The electrochemical corrosion parameters obtained from the polarization curves are given in Table 6.
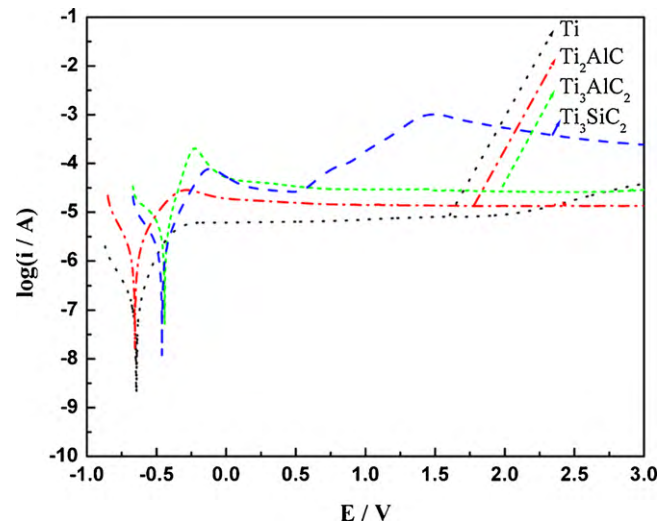
Fig. 8. Polarization curves of Ti, Ti_2AlC, Ti_3AlC_2 and Ti_3SiC_2 in 1 M NaOH solution at the scanning rate of 1 mV/s.

Table 6

Electrochemical parameters obtained from the polarization curves of Ti, Ti$_2$AlC, Ti$_3$AlC$_2$ and Ti$_3$SiC$_2$ in 1 M NaOH solution.

Samples	Corrosion potential (V)	Passivating current density (μA cm^{-2})	Passivating range (V)
Ti	−0.644	5–7	−0.24 to 1.8
Ti$_2$AlC	−0.656	10–20	−0.28 to 3.0
Ti$_3$AlC$_2$	−0.442	20–30	−0.22 to 3.0
Ti$_3$SiC$_2$	−0.460	20–30	−0.11 to 0.6

It can be seen from Fig. 8 that both Ti$_3$AlC$_2$ and Ti$_2$AlC are quite stable in NaOH. The corrosion potential of Ti$_3$AlC$_2$ is ca. 0.21 V higher than that of Ti$_2$AlC (Table 6), implying that the corrosion tendency of Ti$_2$AlC is higher than that of Ti$_3$AlC$_2$. Meanwhile, the passivating range of Ti$_3$AlC$_2$ is larger. Though the passivating current density of Ti$_2$AlC is slightly lower, the difference is not significant. It can thus be concluded that Ti$_3$AlC$_2$ is more stable than Ti$_2$AlC due to the stronger Ti–C bonds in the former.[5]

The passivating range of Ti$_3$SiC$_2$ is much smaller than that of Ti$_3$AlC$_2$. In addition, there is an anodic oxidation peak at ca. 1.5 V on this polarization curve, which is possibly attributed to the oxygen evolution reaction. Moreover, its anodic current density is much higher than that of Ti$_3$AlC$_2$ at potentials higher than ca. 0.6 V. As a result, Ti$_3$AlC$_2$ exhibits better corrosion behavior than Ti$_3$SiC$_2$ at relative higher potential.

The corrosion potential of Ti$_3$AlC$_2$ is also found ca. 0.20 V higher than that of Ti, indicating that the former is more stable. Though the passivating current density of Ti$_3$AlC$_2$ is slightly higher than that of Ti, the current increases at ca. 1.8 V on the polarization curve of Ti which corresponds to oxygen evolution. This implies that the oxygen evolution is inhibited on Ti$_3$AlC$_2$ surface in a wider potential region. Therefore, the changes in the electrical conductivity and the thickness of the passivating film can effectively impede the electron tunneling for the oxygen evolution reaction on Ti$_3$AlC$_2$. Based on the above analyses, we can conclude that Ti$_3$AlC$_2$ shows unique corrosion resistance in 1 M NaOH solution.

5. Conclusions

Ti$_3$AlC$_2$ exhibits excellent corrosion resistance in 1 M NaOH solution due to the formation of two-layer passivating films consisting of mainly titanium oxides. It is further confirmed that Ti$_3$AlC$_2$ shows unique virtues in 1 M NaOH solution compared to some versatile materials.

However, intergranular corrosion occurs when Ti$_3$AlC$_2$ is immersed in 1 M H$_2$SO$_4$ solution or after anodic polarization, which indicates that the long-term corrosion resistance of Ti$_3$AlC$_2$ in H$_2$SO$_4$ is unsatisfactory.

References

1. Barsoum MW, Ali M, El-Raghy T. Processing and characterization of Ti$_2$AlC, Ti$_2$AlN, and Ti$_2$AlC$_{0.5}$N$_{0.5}$. *Metall Mater Trans A* 2000;**31**:1857–65.
2. Wang JY, Zhou YC. Recent progress in theoretical prediction, preparation, and characterization of layered ternary transition-metal carbides. *Annu Rev Mater Res* 2009;**39**:415–43.
3. Eklund P, Beckers M, Jansson U, Högberg H, Hultman L. The M$_{n+1}$AX$_n$ phases: materials science and thin-film processing. *Thin Solid Films* 2010;**518**:1851–78.
4. Jovic VD, Barsoum MW. Electrolytic cell and electrodes for use in electrochemical processes. US Patent 7,001,494 B2; 2006.
5. Jovic VD, Barsoum MW, Jovic BM, Gupta S, El-Raghy T. Corrosion behavior of select MAX phases in NaOH, HCl and H$_2$SO$_4$. *Corros Sci* 2006;**48**:4274–82.
6. Travaglini J, Barsoum MW, Jovic VD, El-Raghy T. The corrosion behavior of Ti$_3$SiC$_2$ in common acids and dilute NaOH. *Corros Sci* 2003;**45**:1313–27.
7. El-Raghy T, Barsoum MW. Preliminary report on the electrochemical behavior of Ti$_3$SiC$_2$. *J Mater Sci Lett* 1999;**18**:519–20.
8. Jovic VD, Barsoum MW. Corrosion behavior and passive film characteristics formed on Ti, Ti$_3$SiC$_2$, and Ti$_4$AlN$_3$ in H$_2$SO$_4$ and HCl. *J Electrochem Soc* 2004;**151**:B71–6.
9. Ren SF, Meng JH, Wang JB, Lu JJ, Yang SR. Tribocorrosion behavior of Ti$_3$SiC$_2$ in the dilute and concentrated sulfuric acid solutions. *Wear* 2010;**269**:50–9.
10. Jovic VD, Barsoum MW, Jovic BM, Ganguly A, El-Raghy T. Corrosion behavior of Ti$_3$GeC$_2$ and Ti$_2$AlN in 1 M NaOH. *J Electrochem Soc* 2006;**153**:B238–43.
11. Wang XH, Zhou YC. Solid–liquid reaction synthesis of layered machinable Ti$_3$AlC$_2$ ceramic. *J Mater Chem* 2002;**12**:455–60.
12. Finkel P, Barsoum MW, El-Raghy T. Low temperature dependencies of the elastic properties of Ti$_4$AlN$_3$, Ti$_3$Al$_{1.1}$C$_{1.8}$, and Ti$_3$SiC$_2$. *J Appl Phys* 2000;**87**:1701–3.
13. Wang XH, Zhou YC. Oxidation behavior of Ti$_3$AlC$_2$ at 1000–1400 °C in air. *Corros Sci* 2003;**45**:891–907.
14. Wen F, Xie CS, Cai SZ, Gui YH. Electrochemical behaviour of copper/LDPE composites in the simulated uterine solution. *Electrochim Acta* 2006;**51**:5606–11.
15. Wu HL, Cheng YL, Li LL, Chen ZH, Wang HM, Zhang Z. The anodization of ZK60 magnesium alloy in alkaline solution containing silicate and the corrosion properties of the anodized films. *Appl Surf Sci* 2007;**253**:9387–94.
16. Sathiyanarayanan S, Azim SS, Venkatachari G. A new corrosion protection coating with polyaniline–TiO$_2$ composite for steel. *Electrochim Acta* 2007;**52**:2068–74.
17. Shibli SMA, George S. Electrochemical impedance spectroscopic analysis of Al–Zn alloy sacrificial anode by RuO$_2$ catalytic coating. *Appl Surf Sci* 2007;**253**:7510–5.
18. Barranco V, Escudero ML, Garcia-Alonso MC. 3D, chemical and electrochemical characterization of blasted Ti$_6$Al$_4$V surfaces: its influence on the corrosion behaviour. *Electrochim Acta* 2007;**52**:4374–84.
19. Zheng YF, Wang BL, Wang JG, Li C, Zhao LC. Corrosion behaviour of Ti–Nb–Sn shape memory alloys in different simulated body solutions. *Mater Sci Eng A* 2006;**438–440**:891–5.
20. Ge HH, Zhou GD, Wu WQ. Passivation model of 316 stainless steel in simulated cooling water and the effect of sulfide on the passive film. *Appl Surf Sci* 2003;**211**:321–34.
21. Metikos-Hukovic M, Kwokal A, Piljac J. The influence of niobium and vanadium on passivity of titanium-based implants in physiological solution. *Biomaterials* 2003;**24**:3765–75.
22. Andrews A, Herrmann M, Sephton M, Machio Chr, Michaelis A. Electrochemical corrosion of solid and liquid phase sintered silicon carbide in acidic and alkaline environments. *J Eur Ceram Soc* 2007;**27**:2127–35.